Tuning Polybenzimidazole Membrane by Immobilizing a Novel Ionic Liquid with Superior Oxygen Reduction Reaction Kinetics

Hui Hou, Alessandro Mariani, Yanpeng Suo, Xinpei Gao, Jürgen Giffin, Christian Rodenbücher, Stefano Passerini,* and Carsten Korte*

ABSTRACT: Protic ionic liquid (PIL) is a promising nonaqueous electrolyte alternative to replacing phosphoric acid for fuel cells operating at temperatures above 100 °C. In this study, the physical and electrochemical properties of stoichiometric and nonstoichiometric PILs are investigated focusing on their acid/base ratio. The study involves a series of PILs, generically indicated as *N*,*N*-diethyl-3-sulfopropane-1-ammonium trifluoromethanesulfonate ([DESPA$^+$][TfO$^-$]), varying from an excess of the proton acceptor (*N*,*N*-diethyl-3-aminopropane-1-sulfonic acid) to an excess of the proton donor (trifluoromethanesulfonic acid, TfOH). Compared to a state-of-the-art electrolyte, i.e., concentrated phosphoric acid, the nonstoichiometric [DESPA$^+$][TfO$^-$] shows superior oxygen reduction reaction kinetics on the investigated Pt catalysts and oxygen permeation ability ($D_{O_2}\cdot c_{O_2}$). [DESPA$^+$][TfO$^-$] with a base-to-acid molar ratio of 1:2 achieves a current density ~10 times larger than that of concentrated phosphoric acid at 110 °C and 0.8 V. Membranes including polybenzimidazole as a host polymer and stoichiometric and nonstoichiometric [DESPA$^+$][TfO$^-$] as the conductive electrolyte exhibit promising properties in terms of thermal stability and conductivity. At 120 °C and 40% relative humidity, conductivities of 2 and 16 mS cm^{-1} are achieved by the membranes employing stoichiometric and excess acid [DESPA$^+$][TfO$^-$], respectively.

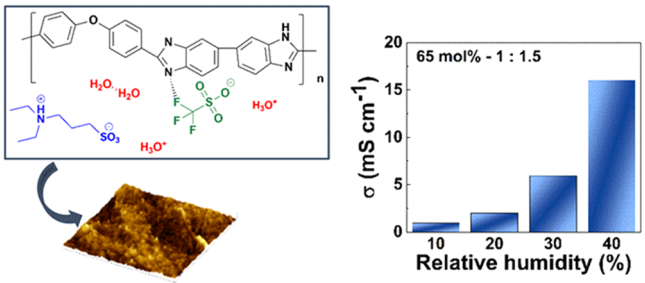

1. INTRODUCTION

In the last few decades, polymer electrolyte fuel cells (PEFCs) have attracted increased research attention as they allow the use of hydrogen as an alternative (chemical) energy storage medium for mobility as well as other applications like spacecraft or marine vessel.[1−3] PEFCs are also of interest due to the rapid depletion of fossil fuel resources that is tied to the current global environmental concerns mainly anthropogenic CO_2 emissions. PEFCs based on proton-conducting membranes consisting of perfluorinated polymers with sulfonic acid moieties (PFSA), e.g., AQUIVION or NAFION, have reached a mature stage of development regarding mobile applications.[4−6] However, due to the limited operational range (up to 80 °C) of PEFCs, they suffer from a number of drawbacks such as large cooling system required, insufficient (if not any) waste heat recovery, and need for a water recirculation/feed gas humidification system.[5,7−10] In fact, the proton conduction of the sulfonated fluorocarbon polymers depends on sufficient swelling with water. The solution to this latter limitation requires an electrolyte (membrane) with a conduction mechanism independent of the presence of high vapor pressure/liquid H_2O.

Several advantages are accompanied when increasing temperature above 100 °C: (i) A more efficient heat management/usable waste heat, (ii) an easier water management as there is no need for humidification of the inlet gas/water recirculation, and (iii) a better CO tolerance in the inlet gas. In the case of a further increase in the operation temperature, some additional disadvantages may occur, e.g., a longer start-up time, higher degradation rates of cell component (carbon corrosion/catalyst support, catalyst degradation), and a much stronger electrolyte dehydration under open-cell conditions.[5,11−16] An operation temperature in the range of 100−120 °C would preserve the advantage and avoid the disadvantages.

Ideal membrane materials for stable and long-term operation at T > 100 °C are polybenzimidazole-type (PBI) polymers.[9,17] Membranes based on PBI and phosphoric acid (H_3PO_4) blends as proton-conducting electrolytes have been the focus of investigations since 1995 and are widely used in high-temperature (HT) PEFCs.[18] They exhibit excellent properties under the designated conditions for HT-PEFC operation (i.e., above 160 °C) owing to their good thermal stability, sufficient

mechanical stability, low gas permeability, and high proton conductivity at very low water vapor pressures.[17,19−21] Experimental studies have shown that a conductivity of 4 × 10^{-2} S cm^{-1} could be achieved at 190 °C for the H_3PO_4/PBI mole ratio of 1:5.[18,22] Nevertheless, a major drawback of using H_3PO_4 as the electrolyte is the sluggish ORR kinetics due to the blocking effect of the catalytic sites and the low oxygen diffusivity and solubility. This results in significantly lower power densities compared to PFSA-based electrolyte membranes.[13,23]

Promising alternatives for nonaqueous electrolytes to H_3PO_4 are ionic liquids (ILs). In general, ILs are compounds that consist of a bulky (organic) cation and large anion with a low charge density, resulting in high lattice energies in the solid state and thus very low melting points. ILs exhibit low volatility and flammability, (often) moderate ionic conductivity, and a wide electrochemical stability window. A subgroup of the ILs are protic ionic liquids (PILs), which consist of a cation or an anion that possesses an exchangeable proton, which can serve as a mobile protonic charge carrier. When PILs are utilized as a nonaqueous electrolyte in PEFCs, high proton conductivity can be achieved. The properties of ILs can be tailored depending on the combination of cationic and anionic moieties which are selected. Among the several advantages of PILs, it is worth stressing that anions of superacids, e.g., TfOH, bis(trifluoromethanesulfonyl)imide (TFSI), and fluoroboric acid (HBF_4), possess the advantage of weak adsorption on the catalysts, resulting in improved fuel cell performance due to the high numbers of free catalytic sites per unit area.[24−27]

Many experimental studies have focused on the development of highly proton-conducting membranes employing different doping electrolytes other than H_3PO_4.[28−31] Van de Ven et al. achieved a conductivity of 1.35 mS cm^{-1} at 129 °C and 1.86 mS cm^{-1} at 190 °C by impregnating a porous PBI membrane into IL 1-H-3-methylimidazolium bis-(trifluoromethanesulfonyl)imide. The proton conductivity of the pristine porous PBI membrane (3 × 10^{-3} mS cm^{-1} at 134 °C and 7 × 10^{-3} mS cm^{-1} at 190 °C) was increased by a factor of 250−450 due to the uptake of the IL.[7] Skorikova et al. proved that introducing an additional PIL into a H_3PO_4-doped PBI membrane is also beneficial to extend the lifetime of the gas diffusion electrode.[32] Nair et al. prepared a membrane by blending poly(vinylidene fluoride-*co*-hexafluoropropylene) (PVDF-HFP) with the PIL diethylmethylammonium trifluoromethanesulfonate ([DEMA][TfO]) and nanosilica modified with $HClO_4$. With a loading of 80 wt % [DEMA][TfO], the blend membrane achieved a maximum conductivity of 0.6 mS cm^{-1} at 100 °C.[33] Wang et al. described the immobilization of 1-hexyl-3-methylimidazolium trifluoromethanesulfonate into a dense PBI membrane. The blend membrane exhibited good performance in terms of thermal stability, mechanical stability, and low methanol crossover.[34] Neves et al. modified a NAFION membrane via immobilization of a certain fraction of IL cations. This led to the discovery of an effective approach to obtain a membrane with tailored properties.[35] Two PILs, i.e., *bis*-(2-ethyl-hexyl)-ammonium hydrogen phosphate ([$EHNH_2$][H_2PO_4]) and imidazolium hexanoate ([Im][Hex]), were immobilized in a poly(vinylidene fluoride) (PVDF) membrane.[36] The blended membranes showed enhanced proton conductivity, 33 mS cm^{-1} for [$EHNH_2$][H_2PO_4]/PVDF and 69 mS cm^{-1} for [Im][Hex]/PVDF at 60 °C, and good mechanical stability.[36]

There are two widely applied methods for preparing blend membranes composed of an IL and a host polymer, namely, swelling and solution casting. Sood et al. investigated the influence of the blending method of NAFION and PILs based on a triethylammonium cation (TEA), leading to the finding that the preparation method has a great impact on the membrane's morphology.[37] The cast membranes have better long-range crystalline order and slightly higher correlation distance in the ionic domains.[37] The morphology also plays an important role with respect to the thermomechanical properties and gas permeability. Cast NAFION membranes with 5−20 wt % TEA-based IL maintain a storage modulus of at least 0.5 MPa, even at 150−190 °C, whereas the swollen membranes with the same composition collapse before reaching 100 °C. Finally, the H_2/O_2 permeability coefficients of cast membranes are smaller by a factor of 1.1−1.4 than those of doped membranes.[37]

In this study, a PIL with a highly acidic cation is investigated based on a potential application as an electrolyte in IT-PEFCs. This type of PIL can be prepared by means of a proton exchange reaction between an organic Brønsted base B and a Brønsted superacid HA, as per eq 1

$$B + HA \rightleftarrows HB^+ + A^- \quad (1)$$

In general, the anion A^- (conjugated base) of a superacid (e.g., TfOH) only has a very small basicity and a negligible nucleophilicity. The acidity of the cation HB^+ depends on the strength of base B. A PIL with high acidity (or proton mobility) offers several advantages for future fuel cell applications. In the case of the presence of (residual) water or of an excess of the base B, a highly acidic PIL will significantly enhance conductivity. The proton can be transferred from the acidic cation to the free base or to the amphoteric water or back to another base molecule, respectively, mimicking the Grotthuss mechanism. Only slight conformational rearrangements of the proton-carrying ions are necessary to enable long-range motion.[27] Besides, in a nonaqueous protic electrolyte, the protons necessary for the cathodic oxygen reduction reaction (ORR) cannot be delivered by the ubiquitous solvent water. In recent kinetic studies on PILs with various cation acidities, it emerged that the proton donor properties of the cation become rate-limiting; thus, it is an important parameter.[38] An acidic PIL can also protonate the alkaline moieties in an ionogene polymer, e.g., a PBI. This will increase the interactions between the IL and the host material as well as help to immobilize the PIL at high levels.

An in-house synthesized PIL, *N*,*N*-diethyl-3-sulfopropane-1-ammonium trifluoromethanesulfonate ([$DESPA^+$][TfO^-]) (see Figure 1), was selected in this study due to its good thermal stability, conductivity, ORR kinetics, and fast oxygen transport, as reported in our previous work.[39,40] Considering the water production and possible leaching of the PIL electrolyte, respectively, of the free acid and base during PEFC operation, an investigation of the PIL/H_2O blends with

various stoichiometric ratios is of particular importance. The stoichiometry of the PIL blend is controlled by mixing the appropriate amount of zwitterionic base and the acid TfOH. The nonstoichiometric PILs mentioned here can be divided into two categories: (i) zwitterionic base is not fully protonated by acid, and the blend contains B, HB^+, and A^-; (ii) acid is not fully neutralized by the base, thus the blend consists of HA, HB^+, and A^- (see eq 1).[41] The properties relevant for a future application in a fuel cell including thermal stability, phase transition behavior, conductivity, and ORR kinetics were investigated. The base-to-acid molar ratio of the PIL blends is varying from 1.5:1 to 1:2.5. As shown in a preceding study, the amount of $[DESPA^+][TfO^-]$ immobilized in the host PBI polymer has a major impact on the cell performance. Thus, the maximum degree of loading in the case of the nonstoichiometric PILs and the influence of the nonstoichiometry on the properties of the blend membranes are evaluated.

2. EXPERIMENTAL SECTION

2.1. Preparation of the Protic Ionic Liquids. All of the chemicals were used as received. The stoichiometric and nonstoichiometric PIL samples were prepared by mixing the calculated amounts of the *N*,*N*-diethyl-3-aminopropane-1-sulfonic acid, with trifluoromethanesulfonic acid (reagent grade, 98%, Sigma-Aldrich), labeled as stoichiometric molar ratios *x*:*y*. A more detailed description of the preparation of the *N*,*N*-diethyl-3-aminopropane-1-sulfonic acid can be found elsewhere.[39,40] The base-to-acid molar ratio *x*:*y* was varied from 1.5:1 to 1:2.5. The water molar fractions of the nonstoichiometric blends were calculated on the basis of theoretical PIL units, e.g., in the case of a blend with a base-to-acid stoichiometry of 1:2, a blend unit B·2 HA is composed of one PIL cation HB^+, an anion A^-, and one molecule of the free acid HA. The water content was adjusted by adding ultrapure water (Millipore) and verified using Karl–Fischer titration (825 KF Titrando, Metrohm).

2.2. Characterization of the Stoichiometric and Nonstoichiometric $[DESPA^+][TfO^-]$ Electrolytes. The thermal behavior of the electrolytes was investigated by means of thermogravimetry analysis (TGA, PerkinElmer STA 6000). The samples were pretreated at 90 °C for 1 h to avoid a release of water during the measurement, followed by a heating program from 50 to 400 °C with a rate of 1 °C min^{-1} in an open quartz glass crucible under N_2 atmosphere with a flow rate of 20 mL min^{-1}. The phase transition behavior was investigated by performing differential scanning calorimetry (DSC, TA Instruments Q2000 equipped with a liquid N_2 cooling system). The samples were sealed hermetically in Al pans and cycled in the range of −140 to 80 °C at a rate of 5 °C min^{-1}. The electric conductivity was determined using a conductometer combined with a frequency analyzer and a thermostatic bath (MMates Italy). The samples were sealed in glass conductivity cells with two platinized platinum electrodes. The cell constant was determined using a 0.01 M KCl solution as a standard. The samples were cycled from 40 to 120 °C and equilibrated for 50 min at each temperature intended for a measurement.

Cyclic voltammetry (CV) measurements and polarization curves of stoichiometric and nonstoichiometric $[DESPA^+][TfO^-]$ electrolytes were carried out using a standard three-electrode cell under O_2 atmospheres. A more detailed description of the setup including the used electrodes is provided in a previous work.[39,40] The oxygen equilibrium concentration c_{O_2} and the diffusion coefficient D_{O_2} in stoichiometric and nonstoichiometric $[DESPA^+][TfO^-]$ were determined using chronoamperometry. The diffusion-controlled current was measured by means of a planar Pt microelectrode with a diameter of 250 μm (99.9%, MaTeck Material Technologie & Kristalle GmbH). The D_{O_2} and c_{O_2} values were measured from the current transients by fitting the Shoup–Szabo equation to the data[42,44]

$$I = -4nFD_{O_2}rc_{O_2}f(\tau) \tag{2}$$

$$f(\tau) = \frac{\pi}{4} + \frac{\pi^{1/2}}{2\tau^{1/2}} + 0.2146e^{-0.7823\tau^{-0.5}} \tag{3}$$

$$\tau = \frac{4D_{O_2}t}{r^2} \tag{4}$$

where *n* denotes the number of transferred electrons, *F* is the Faraday constant, *r* is the radius of the working electrode (WE), and *t* is the elapsed time.

The water content of the stoichiometric and nonstoichiometric $[DESPA^+][TfO^-]$ electrolytes was adjusted in the range of 32–39 mol %. The CVs were recorded with a scan rate of 100 mV s^{-1}, and the polarization curves were plotted with a scan rate of 5 mV s^{-1}. All of the electrochemical properties were measured in the temperature range of 90–120 °C.

2.3. Preparation of the PBI–PIL Blend Membrane. The PBI–PIL blend membranes were prepared by means of solution casting. The PBI solution (O-PBI, Fumion AMLD, PBI polymer solution in DMAc, Fumatech) was dried under air at 80 °C for 3 days, which was followed by drying at 80 °C under vacuum overnight to eliminate the residual DMAc solvent. The ^{13}C NMR and ^1H NMR spectra of the pristine PBI membrane are depicted in Figure S1. The average molar mass of the PBI sample was determined via gel permeation chromatography, and the results are shown in the Supporting Information. The dry PBI was dissolved in dimethyl sulfoxide (DMSO, ≥99.9%, VWR Chemicals) with a ratio of 1:50 (w/w) at 80 °C. An appropriate amount of $[DESPA^+][TfO^-]$ was mixed with the PBI solution to maintain a desired molar ratio (*z* mol %) in the blend membrane. The blend membranes were named in the form of: *z* mol % − *x*:*y*. The PBI–PIL solutions were poured into a Petri dish, and the DMSO solvent was evaporated slowly at 50 °C under air for 2 days, followed by a drying process at 70 °C for 2 days. The residuals of the solvent were removed by a heat treatment in a vacuum oven overnight at 80 °C. An identical process was used for fabricating the blend membranes with the nonstoichiometric PILs (base-to-acid molar ratio of 1:1.5). A schematic sketch of the blend membrane preparation is shown in Figure 2. A visual inspection of the blend membranes allows a rough estimation of the homogeneity. The membrane becomes more inhomogeneous with an increasing amount of the PIL loading. The maximum molar ratio of stoichiometric $[DESPA^+][TfO^-]$ is up to 74 mol % and up to 65 mol % for the nonstoichiometric $[DESPA^+][TfO^-]$ (acid-to-base molar ratio of

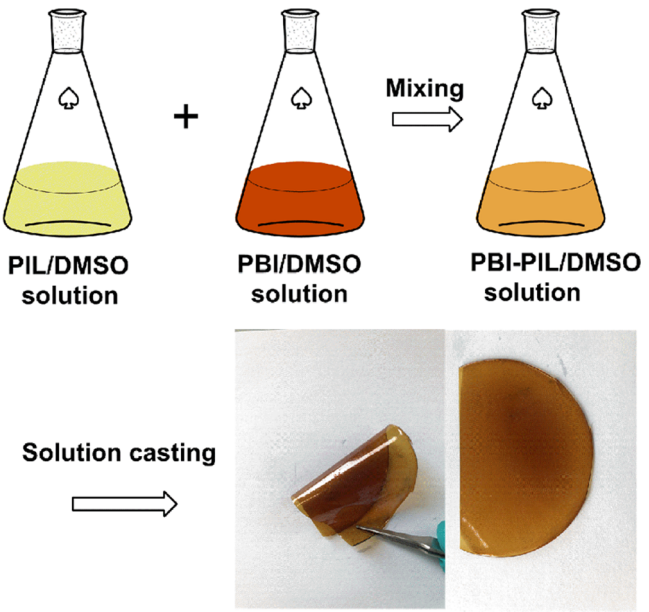

Figure 2. Schematic drawing of the PBI–PIL blend membrane preparation and a photograph of the blend membrane 74 mol %—1:1.

1.5); see also Figure S2. Thus, only the homogeneous membrane samples are characterized in the following.

2.4. PBI−PIL Blend Membrane Characterization. The IR spectra of the PBI−PIL membrane were recorded at ambient temperature by means of an FT-IR spectrometer (Nicolet iS 20 FT-IR spectrometer, Thermo Fisher Scientific GmbH) equipped with an ATR unit using a diamond window (GladiATR single reflection, PIKE Technologies). The through-plane ionic conductivity was measured with an impedance analyzer (Solartron 1260) in a temperature- and humidity-controlled climate chamber (WK3600/40, Weiss Umwelttechnik GmbH). The cell was in-house-designed with a PVDF interior. Strips of the membrane samples with a size of 2 × 1.5 cm^2 were sandwiched between two Pt electrodes with a diameter of 1 mm (99.9%, MaTeck Material Technologie & Kristalle GmbH). The impedance was measured in a frequency range of $1-10^5$ Hz. The conductivity yields as

$$\sigma = \frac{1}{R}\frac{l}{A} \tag{5}$$

where σ is the total ionic conductivity, R is the measured membrane resistance, l is the distance between the electrode, and A is the cross-sectional area of the membrane.[45]

The mechanical properties were measured under ambient conditions using a stress−strain material testing machine (ZwickRoell GmbH & Co. KG). The membrane samples were cut into strips 10 cm in length and 1 cm in width. The elongation rate was set to 5 mm min^{-1}. Each sample was tested three times, and the average value is provided here.

The atomic force microscopy (AFM) images were recorded with a Cypher S (Asylum Research, Santa Barbara) in tapping mode under ambient conditions. The images were processed using the Gwyddion 2.57 software.

The small-angle X-ray scattering (SAXS) patterns of the blend membranes were collected using a Xeuss 3.0c (Xenocs − Grenoble, France) equipped with an Eiger2 1M detector. The wide-angle X-ray scattering (WAXS) patterns were collected using the same setup but equipped with an Eiger2 500k detector. The sample-to-SAXS detector distance was set to 800 mm. A Cu-Kα source was exploited with a beam size of 0.9 × 0.9 mm^2, by which a flux of ~10^8 photons s^{-1} could be obtained. The pattern collected for the direct beam was subtracted in the SAXS patterns as a background. [$DESPA^+$][TfO^-] was injected into a borosilicate capillary (outside diameter 1.5 mm, WJM-Glas/Müller GmbH) and subsequently sealed. The pattern of the empty capillary was also recorded and used in the background subtraction. The instrument's sample chamber was kept under vacuum (p = 15 μbar) during the measurements. Each sample was exposed to the X-ray beam for 10 min to ensure a good signal-to-noise ratio. The data treatment was performed using the SAXSutilities2 software.

3. RESULTS AND DISCUSSION

3.1. Thermal Analysis of the Stoichiometric and Nonstoichiometric [$DESPA^+$][TfO^-] Electrolyte. When performing TGA measurements, the samples with stoichiometry varying from 1.5:1 to 1:1 exhibited a one-step decomposition above 150 °C, indicating a sufficiently high thermal stability. With an increasing amount of excess acid present in the sample, a two-step decomposition process becomes apparent (see Figure 3). The first decomposition steps may be attributed to a loss of TfOH. Taking the sample with a stoichiometry of 1:2 as an example, the first weight loss of 31 wt % in the temperature range of 86−214 °C can be assigned to the loss of the (free) excess TfOH and residue water in the sample. This agrees well with the initial composition of 30 wt % excess TfOH. The second decomposition step starts at 214 °C. The weight loss in the temperature range of 214−392 °C may be caused by PIL decomposition. Up to a temperature of 392 °C, a weight loss of 62 wt % can be observed. This may be explained by the decomposition of the PIL first through re-protonation of the trifluoromethanesulfonate anions and subsequent release of TfOH, then follows the decomposition of the remaining base. Thus, the total weight loss (62 wt %) in the temperature range of 214−392 °C agrees well with the adjusted sample composition of 70 wt % of the bound base and acid. The weight losses of the samples with excess acids are listed in Table S1.

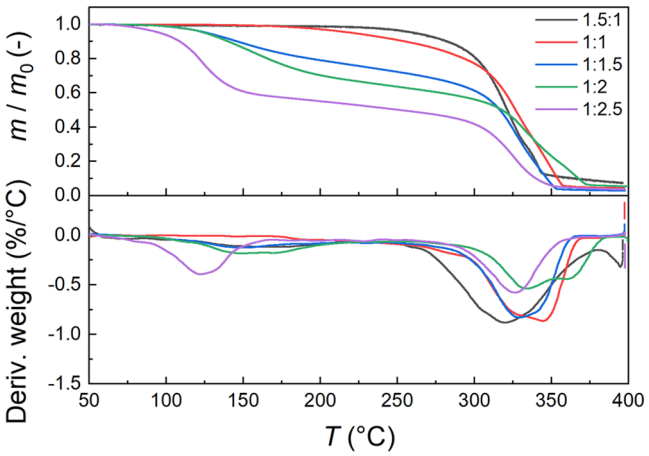

Figure 3. Dynamic TG and DTG curves of base-to-acid with the stoichiometry varied from 1.5:1 to 1:2.5 and a heating rate of 1 °C min^{-1}; the samples were pretreated at 90 °C for 1 h.

Because of water production during PEFC operation, an investigation of the influence of residual water on the PIL electrolyte is necessary. The glass-transition temperatures T_g of the [$DESPA^+$][TfO^-] blends with different stoichiometries are investigated as a function of the molar fraction of water (see Figure 4). The DSC patterns are shown in Figure S3. All of the blends showed no crystallization or melting behavior. Only a glass transition could be observed in the investigated temperature range.

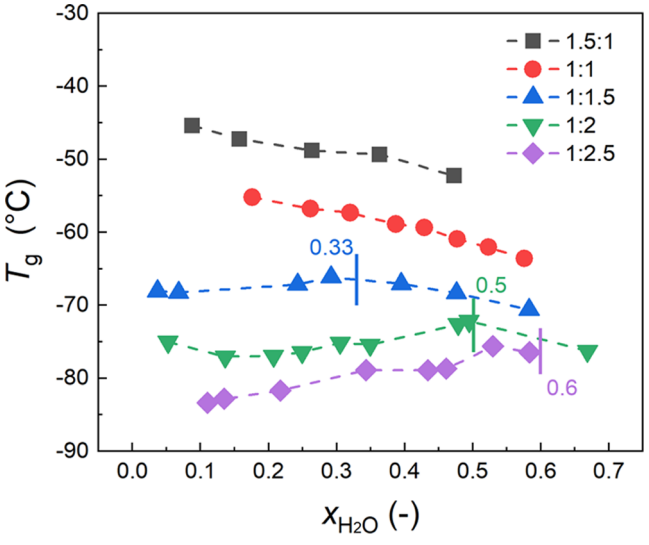

Figure 4. Dependence of the glass-transition temperature on the water molar fraction of [$DESPA^+$][TfO^-] with a stoichiometry from 1.5:1 to 1:2.5. The lines are only for visual guidance.

The glass-transition temperature T_g is influenced by two factors, namely, the amount of free excess acid and the water fraction. In general, T_g is decreasing with an increasing fraction of the excess acid. A similar trend can be observed in blends of 1.5:1 and 1:1 when considering the water influence, i.e., an increasing x_{H_2O} could lead to a decreasing T_g. The influence of water on T_g is different in blends with excess acid. T_g first increases with an increasing water fraction and then decreases again. Taking a blend with a stoichiometry of 1:1.5 as an example, by adding water, the free acid may bond to it. When most of the free acid is bound at a composition of $x_{H_2O} = 0.33$, it corresponds to a (free) excess acid and H_2O molar ratio of 1:1, which accords well with the observed decreasing of T_g when the water fraction exceeds 0.33. A similar trend is observed in other blends with excess acid.

3.2. Conductivity of the Stoichiometric and Non-stoichiometric [DESPA$^+$][TfO$^-$] Electrolytes. The conductivity measurements specify the total conductivity σ of the blends, i.e., the sum of the proton (cation) and anion partial conductivities. The temperature dependence of the conductivity σ of a viscous electrolyte (close to the glass-transition temperature) can be described by the Vogel–Fulcher–Tammann (VFT) equation

$$\sigma = \sigma_0 \exp\left[-\frac{B_\sigma}{R(T - T_0)}\right] \quad (6)$$

where B_σ denotes the pseudo-activation energy, T_0 is the temperature of zero configurational entropy, and σ_0 is the preexponential factor. The conductivity data of all investigated stoichiometries clearly obey a VFT behavior; see Figures 5a and S4a–d. The conductivity is influenced by stoichiometry, temperature, and water content. In the case of the base-excess blends (Figure S5a), the conductivity is enhanced with increasing water content. There is no experimental study regarding the pK_a value of the [DESPA]$^+$, but for an analogue cation 2-sulfoethylmethylammonium, a pK_a value of 0.94 has been estimated in the literature.[38,46] In addition, since the two cations have similar electron density distributions, as shown in Figure S6, assuming a pK_a value of the [DESPA]$^+$ of around zero is reasonable. It is in the same order of magnitude as the hydroxonium cation with a pK_a = 0, which indicates significant protolysis[47,48]

$$(C_2H_5)_2NH^+(CH_2)_3SO_3H + H_2O \rightleftarrows (C_2H_5)_2NH^+(CH_2)_3SO_3^- + H_3O^+ \quad (7)$$

As was illustrated in our previous work, in the case of the stoichiometric [DESPA$^+$][TfO$^-$] being neat or slightly moist ($x_{H_2O} < 0.25$), the proton transfer may be mainly dominated by a vehicular mechanism.[39,40] At a higher water concentration, more proton acceptor species (water, free base) are provided. The contribution to the conductivity via the cooperative mechanism may increase. As is depicted in Figure 5b, the conductivity increases with increasing water molar fraction.

In the case of the excess acid blends, water will also serve as a proton acceptor. Depending on the water fraction, it can be either protonated by the highly acidic excess acid (TfOH) or by the [DESPA]$^+$ cation; see eqs 7 and 8

$$CF_3SO_3H + H_2O \rightleftarrows CF_3SO_3^- + H_3O^+ \quad (8)$$

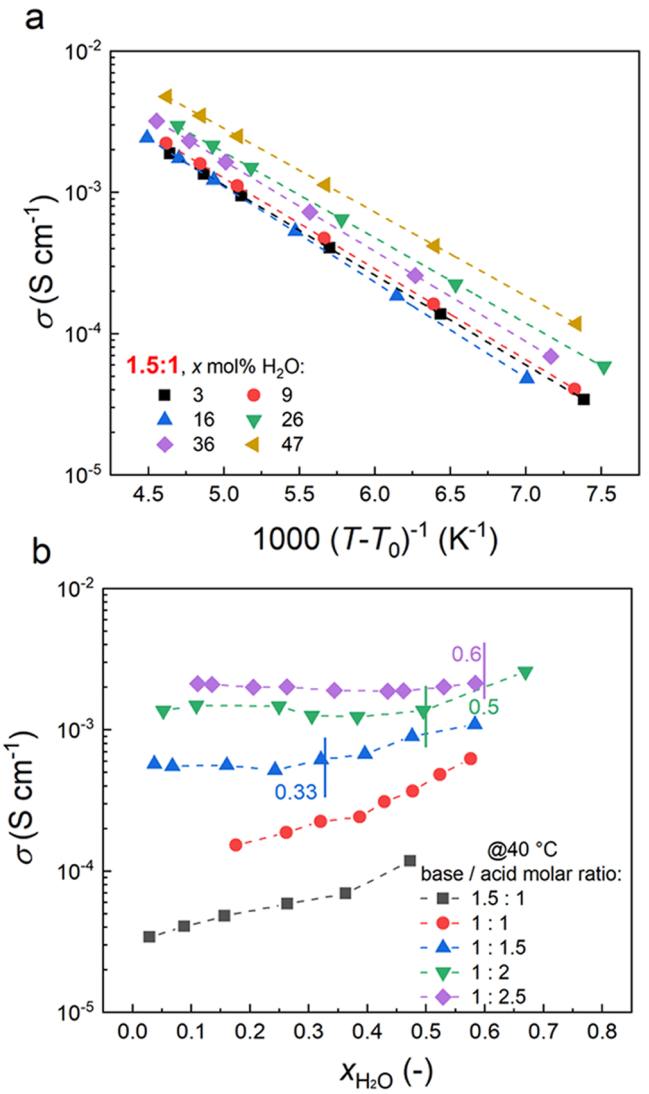

Figure 5. (a) Specific conductivity vs 1000(T – T_0) ^{1} of the nonstoichiometric blend with a base/acid molar ratio of 1.5:1. The symbols represent the experimental data, and the broken lines correspond to the linear fitting, with $R^2 \geq 0.9999$; (b) dependence of conductivity on the water molar fraction in blends with a base-to-acid stoichiometry from 1.5:1 to 1:2.5 at 40 °C. The lines are not fitting and are only a visual reference.

The proton transfer becomes more efficient, either via a vehicular or cooperative mechanism with an increasing water fraction. More importantly, the proton can propagate through the chain that coordinates with hydronium ions and the neighboring [TfO]$^-$ anions.

When plotting the total conductivity σ at a constant temperature vs water fraction, the blends with an excess acid exhibit a distinct plateau for the σ values when reducing the water fraction below a certain value, as can be seen in Figure S5c–e. Taking the blend with a stoichiometry of 1:1.5 as an example, a plateau can be observed at $x_{H_2O} < 0.33$. When the molar fraction of water is higher than 0.33, the conductivity is increasing again. Adding water only has a limited influence on the total conductivity when $x_{H_2O} < 0.33$. Even in the presence of a larger amount of the proton-conductive species, the conductivity does not significantly increase. The positive

influence may be counteracted by the increased viscosity and the electrophoretic and relaxation effects.[49]

3.3. Electrochemical Properties. According to the thermal analysis results shown in Figure 3, the nonstoichiometric [DESPA$^+$][TfO$^-$] with a base-to-acid molar ratio of 1:2.5 shows a clear weight loss starting from 90 °C. Therefore, the electrochemical measurements were only performed with PILs with a base-to-acid molar ratio varying from 1:1 to 1:2.

The open-cell voltage (OCV) was determined by directly measuring the cell voltage at j = 0 using the potentiostat/impedance analyzer as a voltmeter with a high internal resistance. An OCV of 1.05 V can be measure for a Pt cathode at 90 °C under O_2-saturated conditions vs Pd-H using a stoichiometric [DESPA$^+$][TfO$^-$] electrolyte. Under the same conditions, values of 1.07 and 1.10 V can be measured for the blends with base-to-acid stoichiometries of 1:1.5 and 1:2, respectively. A similar trend can be observed at other experimental temperatures (100−120 °C). The OCV can be regarded as a rough indicator for the electrocatalytic activity, i.e., the higher the electrocatalytic activity, the higher OCV can be achieved and the closer to its Nernst potential.[38] The polarization curves for the blends with a stoichiometry varied from 1:1 to 1:2 were recorded in the temperature range of 90−120 °C by scanning the potential in the negative direction from OCV to a potential where the limiting current density was reached. The results are depicted in Figure 7a. The ORR onset potential shifts significantly in the positive direction with an increasing temperature or when adding an excess of TfOH; see Figures 6 and 7a. An excess of TfOH accelerates the proton

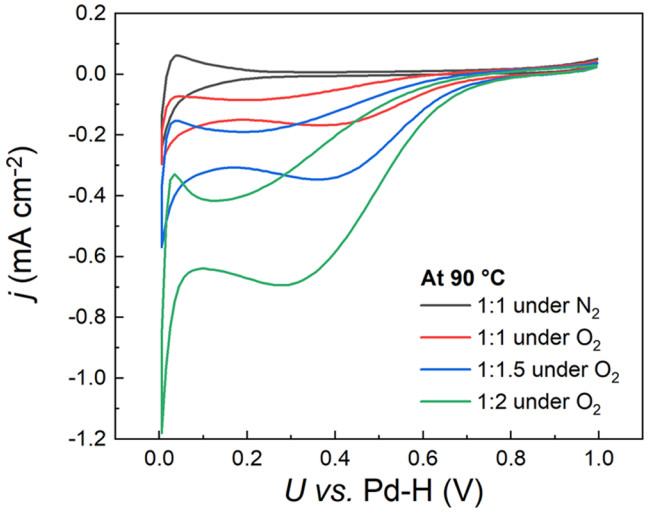

Figure 6. Cyclic voltammograms in blends with a base-to-acid stoichiometry of 1:1 to 1:2 under a N_2 or O_2 atmosphere at 90 °C, with a scan rate of 100 mV s^{-1}.

transfer to O_2, thus boosting the overall ORR kinetics. The significant shift of the ORR onset potentials in the blends with an excess TfOH could be explained by a change of the proton donor species, from H_3O^+ and [DESPA]$^+$ (pK_a = 0) to superacid TfOH (pK_a = −14), as per eq 9. A similar effect in [DEMA][TfO] blends was observed by Goodwin et al.[50] The ORR onset potential is shifted in the positive direction by 0.8 V when adding the acid in neat PIL.

$$1/2\ O_2 + 2\ e^- + TfOH \rightarrow 2[TfO]^- + H_2O \quad (9)$$

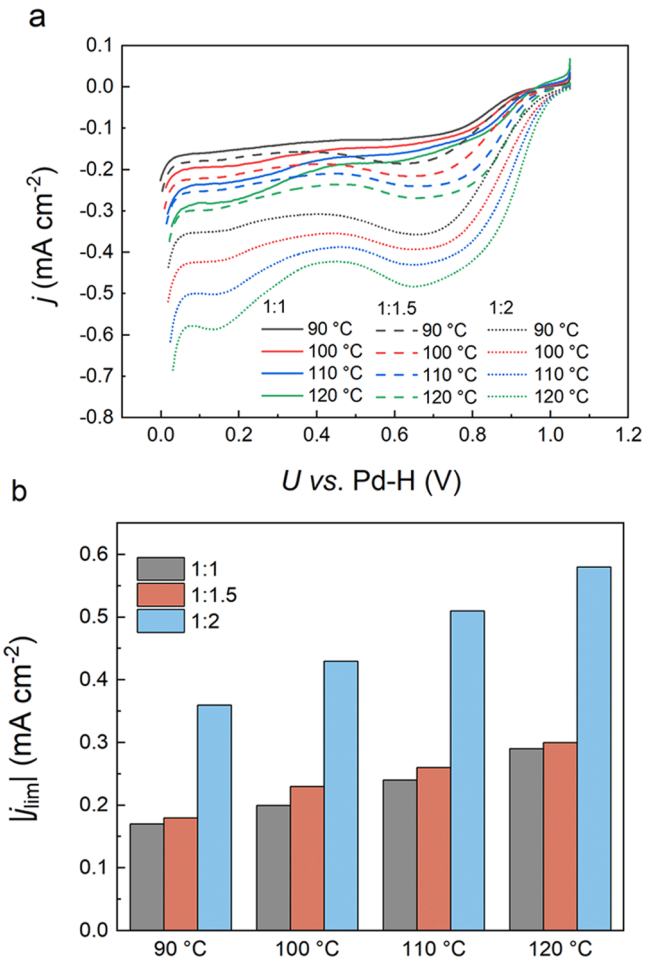

Figure 7. (a) Polarization curves with a scan rate of 5 mV s^{-1} and (b) limiting current density in O_2-saturated blends with a base-to-acid stoichiometry of 1:1 to 1:2.

Compared with the state-of-the-art electrolyte, concentrated H_3PO_4, a current density is achieved of 0.037 mA cm^{-2} at a potential of 0.8 V (vs Pd-H) and 110 °C.[27] Under the same conditions, stoichiometric and nonstoichiometric [DESPA$^+$][TfO$^-$] yield values of 0.15 mA cm^{-2} (base-to-acid molar ratio of 1:1), 0.2 mA cm^{-2} (1:1.5), and 0.37 mA cm^{-2} (1:2). This is obviously a pronounced improvement in the presence of stoichiometric and nonstoichiometric [DESPA$^+$][TfO$^-$].

The value of the oxygen diffusion coefficient D_{O_2} and equilibrium solubility c_{O_2} in the blends with a stoichiometry varying from 1:1 to 1:2 are compiled in Table S2. The product of D_{O_2} and c_{O_2} and thus the O_2 permeability increases with increasing temperature and with increasing excesses of TfOH; see Figure 8. This correlates well with the measured limiting current densities $|j_{lim}|$; see Figure 7b. The O_2 permeability $D_{O_2}\cdot c_{O_2}$ in the 1:2 blend at 90 °C achieves an ∼5 times higher value compared to the 1:1 blend. All blends showed a significantly enhanced $D_{O_2}\cdot c_{O_2}$ compared to concentrated H_3PO_4, e.g., 98% H_3PO_4 has a value of 1.05 × 10^{-12} mol cm^{-1} s^{-1} at 100 °C.[51]

3.4. Thermal Analysis of the PIL−PBI Blend Membrane. A sufficient thermal stability of the PBI−IL blend membrane is crucial for application as an electrolyte in PEFCs above 100 °C. The thermal stabilities of the PIL, pristine PBI, and blend membranes are depicted in Figure 9.

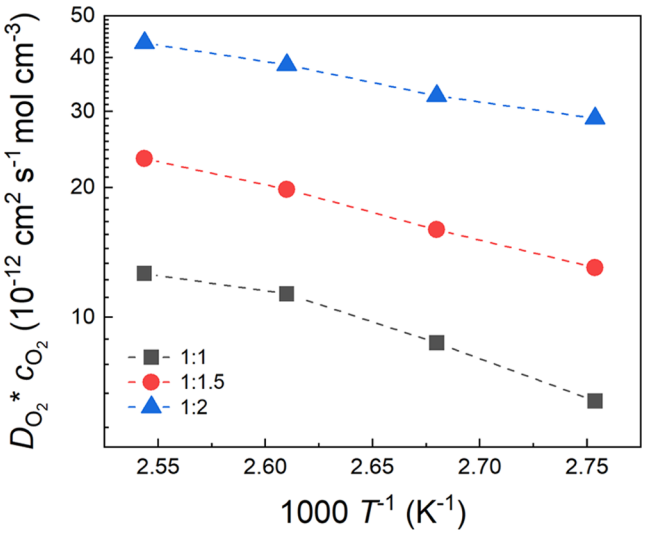

Figure 8. Temperature dependences of the product of $D_{O_2} \cdot c_{O_2}$ in blend electrolytes with a base-to-acid stoichiometry varied from 1:1 to 1:2.

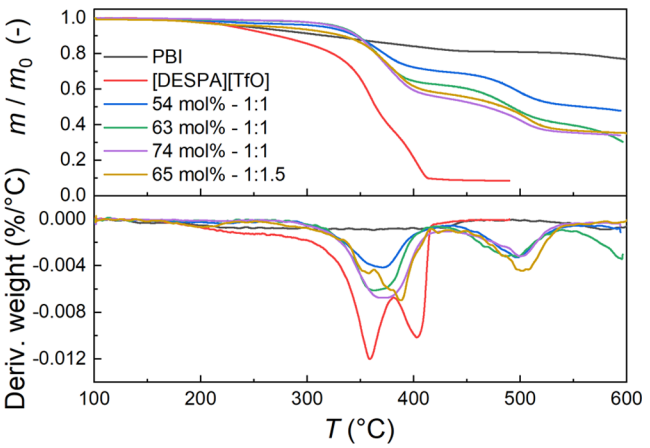

Figure 9. Dynamic TG and DTG curves of the [DESPA$^+$][TfO], pristine PBI, and blend membranes. The heating rate was 10 °C min ^{1}. The membranes were pretreated at 100 °C for 30 min to reduce the influence of water.

The PBI blend membranes showed improved thermal stability compared to [DESPA$^+$][TfO$^-$]. The weight loss near 100 °C could be ascribed to a loss of water. Given that the PBI samples were blended with stoichiometric [DESPA$^+$][TfO$^-$], the second decomposition step occurred between 285 and 550 °C. With respect to the thermal behavior of the stoichiometric PIL, the decomposition was presumably caused by the loss TfOH (back-transfer of the proton from [DESPA]$^+$ and from the imidazolium moieties of the PBI) and by the decomposition of the remaining free base. Most of the immobilized [DESPA$^+$][TfO$^-$] decomposes below 550 °C. This assumption is in line with the initial sample composition (see Table S3). The PBI backbone degrades above 600 °C. The PBI samples blended with the nonstoichiometric PIL exhibited a clear weight loss (about 3 wt %) in the temperature range of 157−244 °C, which could be attributed to the evaporation of a part of the excess acid (see Table S4). All investigated blend membranes showed sufficient thermal stability in the operating temperature range (100−120 °C).

3.5. ATR-IR. The ATR spectra of the free base, [DESPA$^+$][TfO$^-$], the pristine PBI membrane, and the PBI−PIL blend membranes are depicted in Figure 10. In the spectrum of the

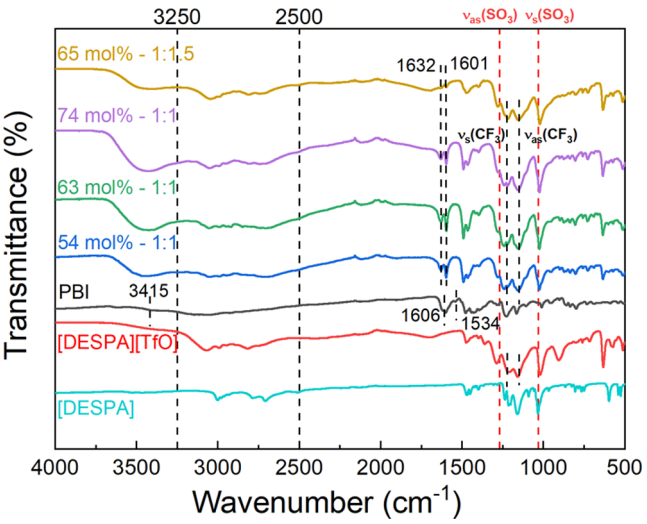

Figure 10. ATR-IR spectra of the free *N*,*N*-diethyl-3-aminopropane-1-sulfonic acid, [DESPA$^+$][TfO], pristine PBI, and the blend membranes.

pristine PBI, the bands present in the region between 4000 and 2000 cm^{-1} can be assigned to the stretching vibration modes of N−H, O−H, and C−H. The characteristic band at 3415 cm^{-1} is due to the isolated N−H stretching mode of the PBI imidazole moiety, i.e., a free N−H group. The bands at 3250−2500 cm^{-1} appear in the range that can be assigned to the stretching mode of the self-associated N−H bonds.[34,52−54] The broad bands become stronger in the blend membrane samples, which may indicate a protonation of the imidazole ring by [DESPA$^+$][TfO$^-$].[54] Similar spectra were also observed in H_3PO_4-doped PBI membranes.[55] The band at 1606 cm^{-1} corresponds to the aromatic C═N stretching mode of PBI and at 1534 cm^{-1} to the aromatic C−C stretching mode of the imidazole ring. These bands are stronger with the presence of the PIL in the PBI matrix and shift toward higher wavenumbers of 1632 and 1601 cm^{-1}, respectively. This could be due to the protonation of the imidazole ring.[52,54] No studies are available in the literature focusing on investigations by vibrational spectroscopy on [DESPA$^+$][TfO$^-$]. Thus, the literature data on other triflate-based ILs are used for comparison.[54,56] The bands located at 1270 and 1032 cm^{-1} are assigned to the asymmetric and symmetric SO_3 stretching modes. The asymmetric and symmetric stretching modes of CF_3 are present at 1149 and 1222 cm^{-1}.[56,57]

3.6. Conductivity of the PIL−PBI Blend Membranes. In addition to the ORR kinetics, conductivity is one key parameter for assessing the fuel cell's performance.[58] To conduct a general evaluation of the PIL loading, water, and temperature influences on the conductivity, the blend membranes were measured from low to high relative humidity (10−40% RH) in the temperature range of 80−120 °C.

The temperature dependence of the total conductivity can be described by the Arrhenius equation, as is conveyed in eq 10

$$\sigma = \frac{\sigma_0}{T} \exp\left[-\frac{E_a}{RT}\right] \quad (10)$$

where E_a is the activation energy for the proton conduction, σ_0 is the preexponential factor, and R is the ideal gas constant. The activation energy is an indicator of the energy required to perform the (rate-limiting) elementary step of the conduction mechanism.[59]

The conductivity is improved by increasing the temperature or relative humidity. It is decreased with an increasing PBI molar fraction, as is depicted in Figure 11a,b. Moreover, Figure 11b clearly suggests that the excess acid in the blend membrane brings a significant improvement in conductivity. At 120 °C and 10% RH, the conductivity of the blend membrane (74 mol %−1:1) exhibits a value of 9.1×10^{-5} S cm^{-1}, in the blend membrane (65 mol %−1:1.5) of 9.5×10^{-4} S cm^{-1} under the same experimental conditions. The conductivity increases by 1 order of magnitude.

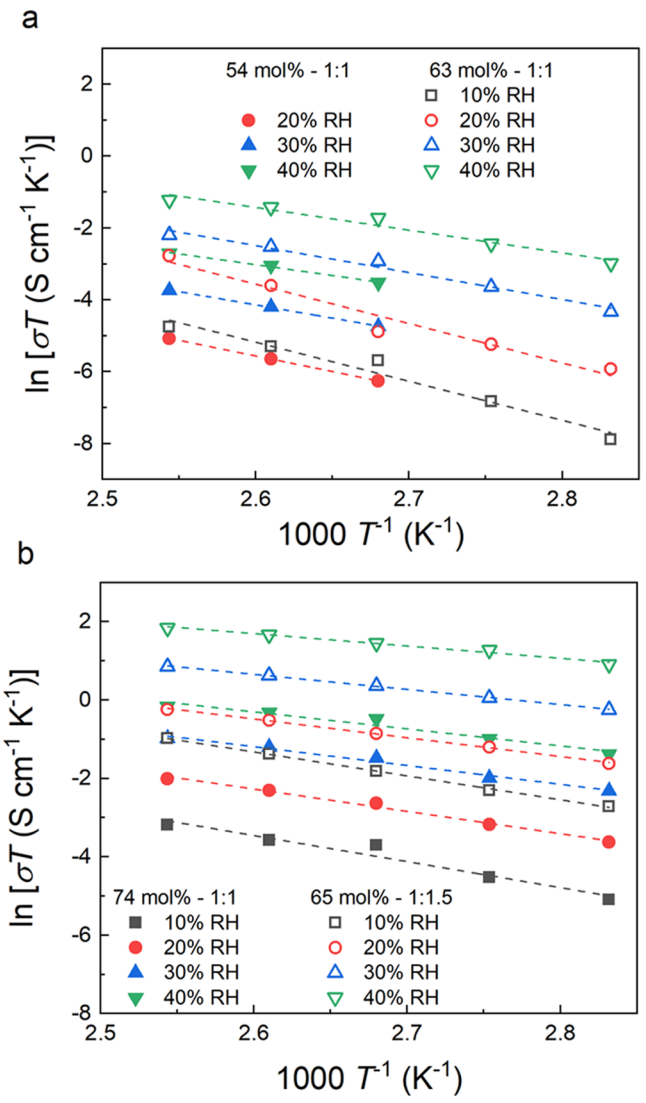

Figure 11. Temperature−conductivity dependence of blend membranes with (a) stoichiometric PIL loading of 54 and of 63 mol % and with (b) stoichiometric PIL loading of 74 mol % and a non-stoichiometric PIL loading of 65 mol %.

The $[TfO]^-$ anions can interact with the PBI's imidazole rings (N−H). Depending on the PIL/PBI ratio and the stoichiometry of the PIL (acid excess), hydronium ions (H_3O^+) are formed due to the protolysis equilibrium in the presence of the water. The proton can move through the H-bond network, as depicted in Figure 12. Furthermore, a vehicular mechanism is possible via the movement of the proton-carrying ions, i.e., $[DESPA]^+$ and H_3O^+.[5,34,59−62] The proton conduction in the blend membrane under humidified conditions may follow a cooperative mechanism and support by means of a vehicular mechanism. However, considering only the results from this study, it is difficult to specify the contribution of these two mechanisms and further investigation is necessary. Moreover, the PIL may also act as a plasticizer that is beneficial to the flexibility of the PBI backbone.[34]

The activation energies for proton conduction in the blend membranes are depicted in Figure 13. In general, E_a decreases with increasing PIL loading. This indicates that a decreasing density of the polymer network due to a higher PIL fraction causes higher mobility among the proton-carrying ions. Increasing humidity (RH%) also has a positive effect on proton conduction. This can be explained by the increasing amount of H_3O^+ due to a protolysis with water, as discussed for the neat PILs. This is beneficial to proton conduction because a cooperative transport mechanism is possible, and the proton may move along a network of the H-bond chains formed by H_3O^+ and H_2O. Moreover, considering the geometry factor, H_3O^+ may diffuse faster than $[DESPA]^+$, which could also lead to faster vehicular transport. The membrane samples with an excess of TfOH exhibit the lowest values of E_a compared to other blend membranes under the same conditions. In the case of the membrane sample 65 mol %−1:1.5, a value of only 26.1 kJ mol^{-1} is measured at 120 °C and 40% RH. The incorporation of TfOH in the blend membrane may have a positive influence on the formation of a domain structure of the polymer and the incorporated PIL by forming H bonds to $[DESPA]^+$ and $[TfO]^-$.[63] Both may significantly accelerate proton transport.

3.7. Stress−Strain Test. The lifetime of a polymer electrolyte fuel cell is not only influenced by the chemical degradation of the catalyst and membrane but also by the latter's mechanical failure. Performing stress−strain tests, all blend membranes exhibit a higher elongation compared to the pristine PBI membranes. The results of this are listed in Table 1. From the literature, it is known that PBI membranes with a high degree of H_3PO_4 doping also suffer losses of mechanical stability.[64] When introducing the acidic PIL into the PBI membrane, an analogous deterioration of the mechanical properties can be observed.

3.8. Characteristic Features of the Membrane Morphology. To gain insight into the surface morphology and homogeneity, a blend membrane (74 mol %−1:1) was investigated by means of tapping-mode AFM. The maps of the topography and the relative phase are depicted in Figure 14 for two different magnifications. The topography map in Figure 14a reveals that the surface can be considered macroscopically flat, with an RMS roughness value of 1.8 nm, but on the nanoscale, a characteristic pattern of randomly oriented grooves is present. In the map (Figure 14d) with higher magnification, it becomes evident that these grooves have a width of several hundred nanometers and a depth of 1−2 nm. Furthermore, also deeper, round depressions with a diameter of 100 nm to 1 μm and depths of 5−10 nm can be identified. The phase maps, which reflect the difference in the interaction between the tip and surface, thus indicating a material contrast, e.g., due to a different hardness,[65] show that the depressions in

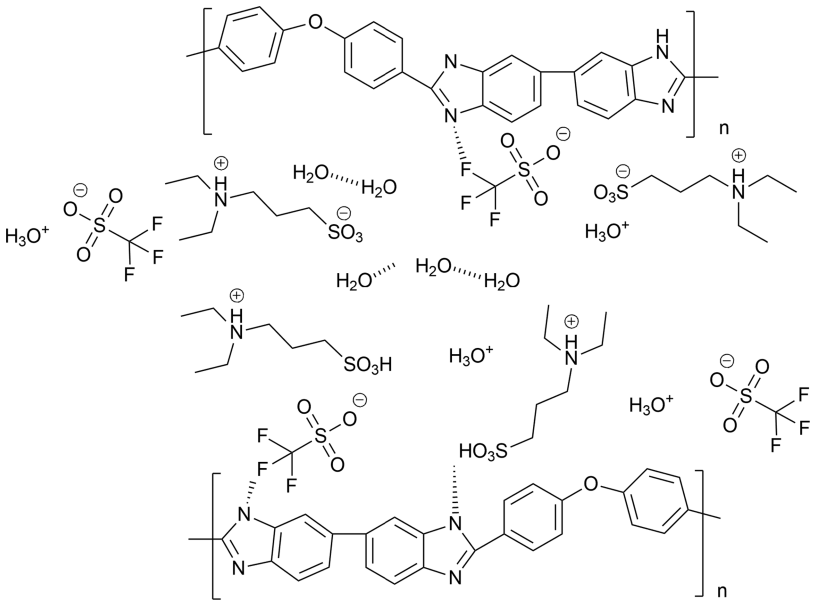

Figure 12. Hypothesis of the IL channel in PBI blend membranes immobilized with stoichiometric [DESPA$^+$][TfO$^-$].

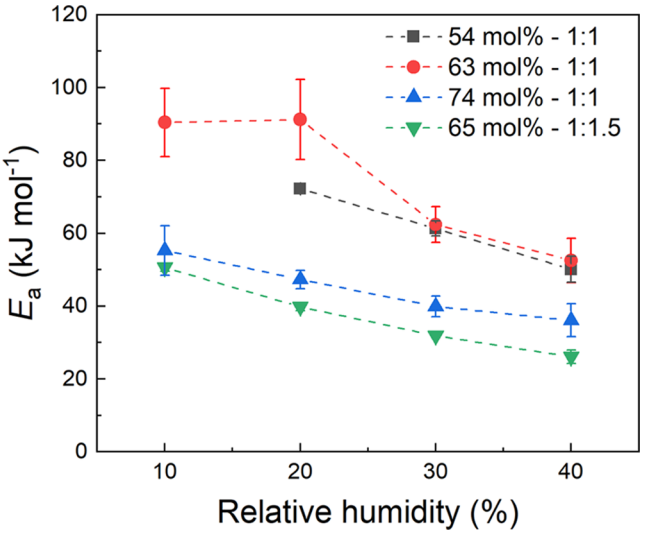

Figure 13. Arrhenius activation energies E_a for the blend membranes obtained from the conductivities displayed in Figure 11. The depicted uncertainty was calculated from the fitting in eq 10. The lines are visual guidelines.

Table 1. Mechanical Properties of the Pristine PBI and the Blend Membranes with a Stoichiometric PIL Loading Varied from 54 to 74 mol % and a Blend Membrane with a Nonstoichiometric PIL (Base-to-Acid Molar Ratio of 1:1.5) Loading of 65 mol %

membrane	Young's modulus (MPa)	ultimate tensile strength (MPa)	elongation at break (%)
pristine PBI	177.5 ± 25.0	151.8 ± 14.7	65.5 ± 7.6
54 mol % − 1:1	21.5 ± 3.5	71.3 ± 8.1	184.0 ± 5.4
63 mol % − 1:1	8.7 ± 2.3	24.8 ± 6.0	188.7 ± 11.0
74 mol % − 1:1	6.6 ± 0.6	23.7 ± 4.8	260.3 ± 9.8
65 mol % − 1:1.5	8.7 ± 2.1	13.8 ± 2.9	125.9 ± 11.6

topography correspond to a higher phase; see Figure 14b and the line profiles in Figure 14c. Also, on other positions on the surface, an increase in the phase beside the grooves can be identified; see Figure 14e,f. It can be concluded that the surface has a certain degree of inhomogeneity, which could indicate the formation of clusters or channels consisting of soft PIL-rich material embedded in the hydrophobic PBI matrix.

As it is visible to the naked eye, all of the blend membranes appear similar at ambient pressure. When applying vacuum, the appearance of the blend membranes with high PIL loading (74 mol %−1:1 and 70 mol %−1:1) is changed; see Figure 15. The blend membrane (70 mol %−1:1) shrinks, and the surface takes on a dry and brittle appearance. Cracks are visible. When the PIL loading is increased to 74 mol %, the membrane seems to leach out the PIL and a wormlike droplet structure can be observed on the surface. However, the samples, 70 mol %−1:1 and 74 mol %−1:1 revert to their original appearance when the vacuum is broken, which indicates the reversibility of the process.

The SAXS and WAXS patterns of the PIL, pristine PBI, and blend membranes are depicted in Figure 16a,b. The characteristic $I(q)$ in low-q regions (at 0.03 Å^{-1}) change with the PIL contents; see Figure 16. It disappears in the pristine PBI and the 54 mol %−1:1 sample and reaches a maximum in the 63 mol %−1:1 sample. When increasing the PIL loading beyond 63 mol %, it decreases again. This is generally associated with a crystallization of the polymer backbone (intercrystalline domains).[66−69] At high q values of 0.25 Å^{-1}, a characteristic peak appears when adding the PIL to the host polymer. This is attributed to side-chain aggregation (cluster domain) and corresponds to the size of the hydrophilic channels.[59,66,68,70] The ionomer peak shifts from 0.258 to 0.206 Å^{-1} when increasing the PIL content (from 54 to 74 mol %) and the characteristic size of the cluster domain changes from 2.434 to 3.048 nm as expected; see Table 2. The peak becomes less recognizable for the samples, 70 mol %−1:1 and 74 mol %−1:1. This may be explained by the crystallization of the polymer and leaching out of the PIL; see Figure 15 (C4 and C5).

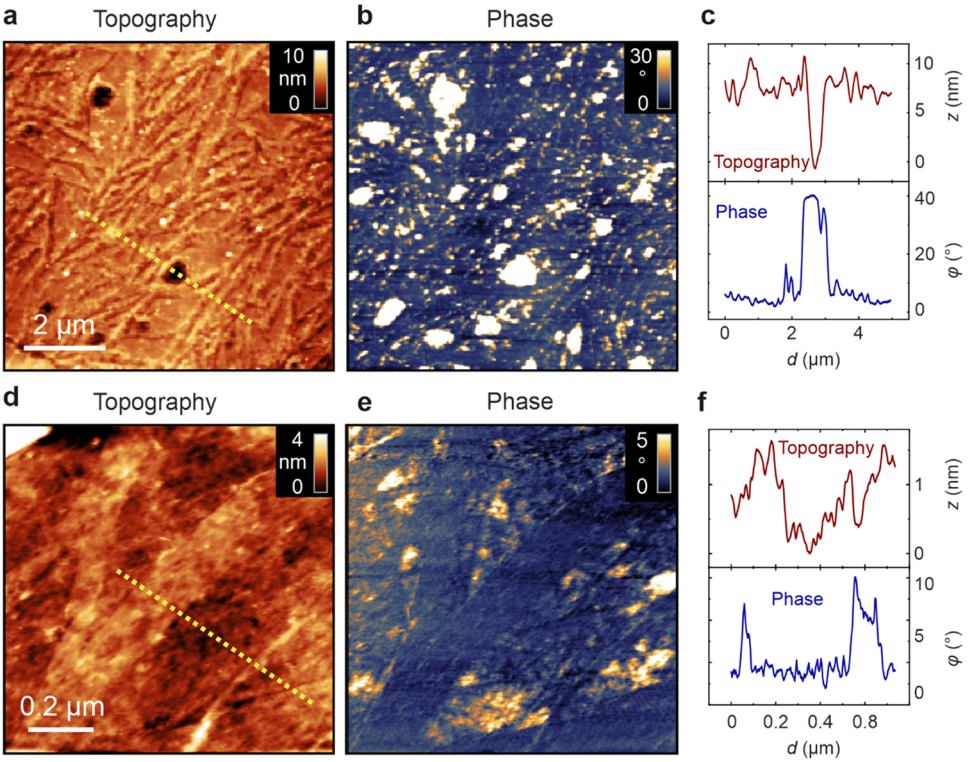

Figure 14. Tapping-mode AFM analysis of the blend membrane: 74 mol %−1:1. Maps of topography and phase with a representative line profile for a 7 × 7 μm^2 scan (a–c) and for a 1 × 1 μm^2 scan (d–f).

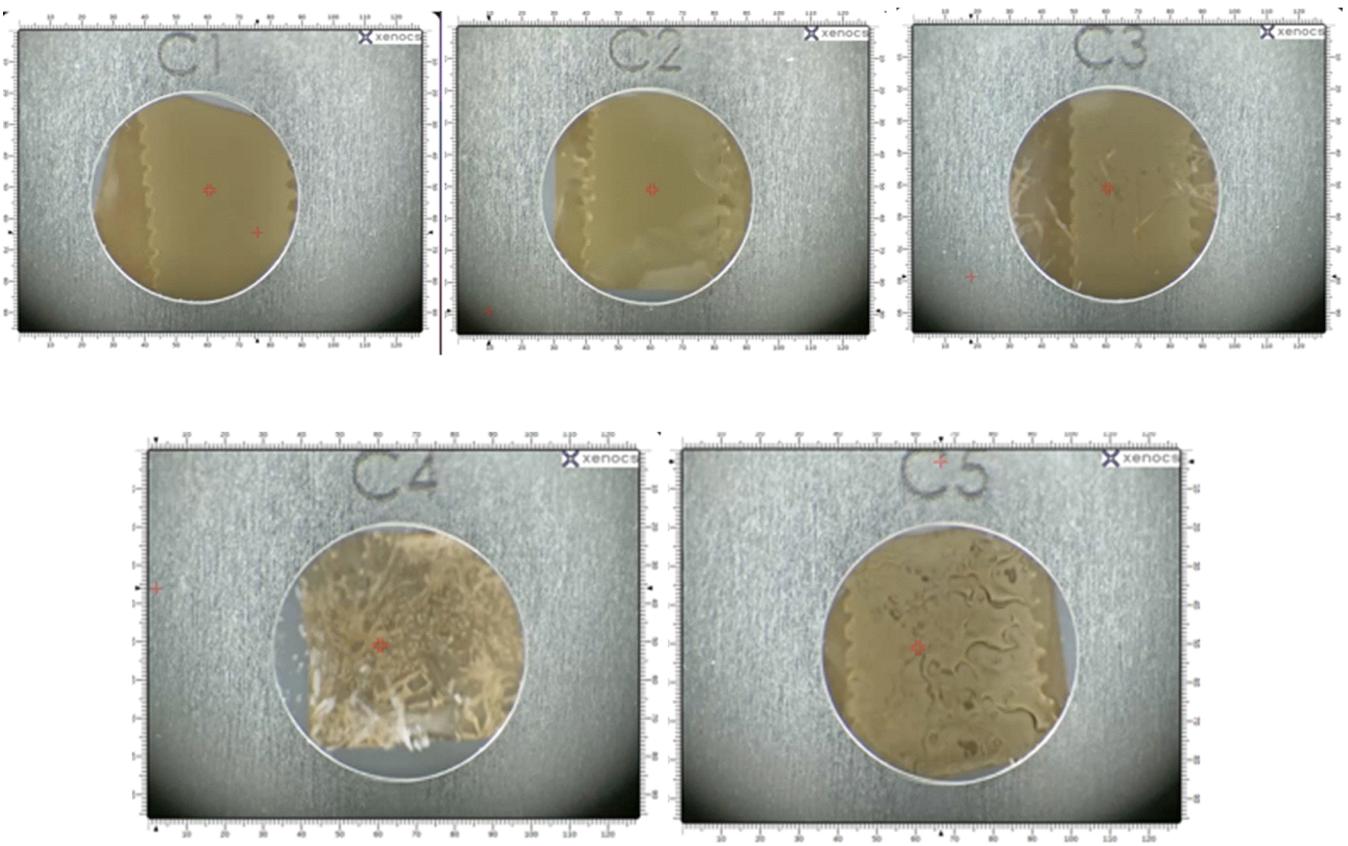

Figure 15. Photographs of the blend membranes in the SAXS instrument sample chamber (p = 15 μbar). C1: pristine PBI; C2: sample 54 mol %−1:1; C3: sample 63 mol %−1:1; C4: sample 70 mol %−1:1; C5: sample 74 mol %−1:1.

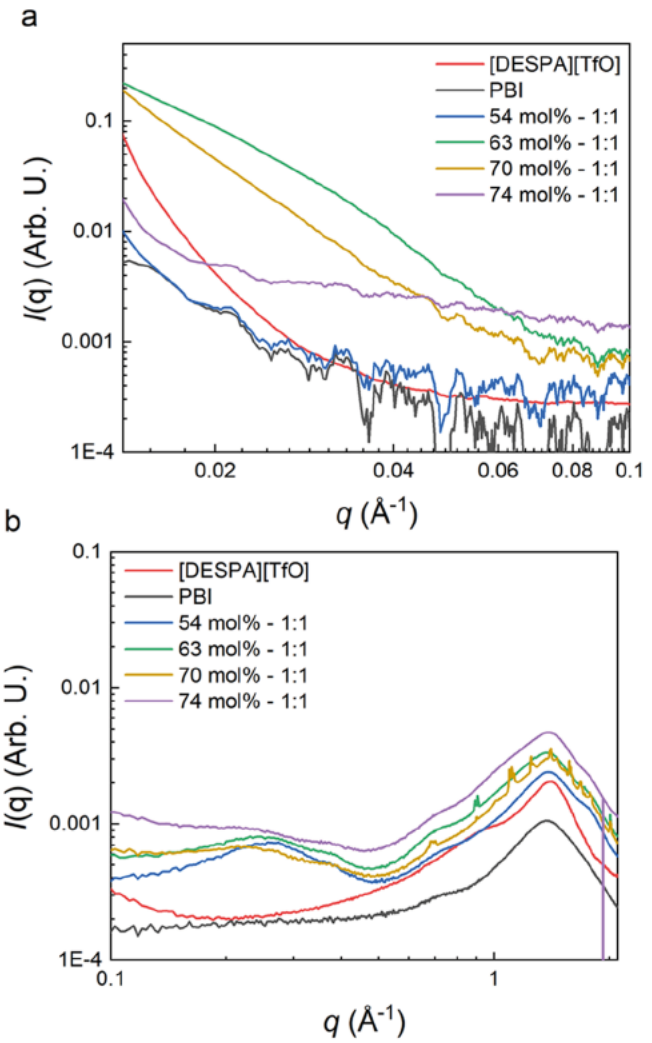

Figure 16. (a) SAXS patterns and (b) WAXS patterns of the pristine PBI, blend PBI membranes, and [DESPA$^+$][TfO$^-$].

Table 2. Characteristic Peak Positions of the Blend Membranes and Typical Size of the Ionic Cluster

membrane	ionomeric peak position (Å^{-1})	characteristic size (nm)
54 mol %−1:1	0.258	2.434
63 mol %−1:1	0.246	2.553
70 mol %−1:1	0.233	2.695
74 mol %−1:1	0.206	3.048

4. CONCLUSIONS

In this study, stoichiometric and nonstoichiometric samples of the PIL, *N,N*-diethyl-3-sulfopropyl-ammonium trifluoromethanesulfonate [DESPA$^+$][TfO$^-$], were prepared and their physical and electrochemical properties were evaluated. An excess of the base, *N,N*-diethyl-3-aminopropane-1-sulfonic acid, enhances the thermal stability and an excess of trifluoromethanesulfonic acid is beneficial to the proton conduction, ORR kinetics, and oxygen permeation. The physical and electrochemical analysis offers a promising prospect by adding an excess of acid to a PIL for use in future PEFCs at elevated operating temperatures.

PBI blend membranes may play a key role in developing PEFC applications operating at 100−120 °C. Blend membranes based on stoichiometric and nonstoichiometric PIL electrolytes were prepared via solution casting. In general, the conductivity and mechanical stability relate to the immobilized amounts of PIL. A large amount of PIL is advantageous in terms of conductivity but results in a loss of mechanical stability. Moreover, the morphology of the blend membrane is significantly influenced by the amount of PIL that is utilized. This study opens the possibility of applying highly acidic PILs that have been immobilized in a host polymer to future fuel cell applications.

■ ASSOCIATED CONTENT

● Supporting Information

The Supporting Information is available free of charge at https://pubs.acs.org/doi/10.1021/acs.chemmater.1c03819.

^{13}C NMR and ^{1}H NMR spectra of the PBI in DMSO-d_6, photographs of PBI blend membranes, molar mass of PBI sample, calculated weight loss from TG curves of samples with a stoichiometry (*x*:*y*) from 1:1.5 to 1:2.5, DSC heating traces of stoichiometric [DESPA$^+$][TfO$^-$] with varied water molar fractions, conductivity dependence on water molar fractions in blends with a base-to-acid stoichiometry from 1:1 to 1:2.5 in the temperature range of 40−120 °C, electron density distributions of the [DESPA$^+$] and [2-Sema$^+$] cations, value of the oxygen diffusion coefficient and solubility in the blends, calculated weight loss of the pristine PBI and PIL−PBI blend membranes from the TG curves, and leakage tests of the PIL−PBI blend membranes (PDF)

■ AUTHOR INFORMATION

Corresponding Authors

Stefano Passerini − *Helmholtz Institute Ulm (HIU), 89081 Ulm, Germany; Karlsruhe Institute of Technology (KIT), 76021 Karlsruhe, Germany;* orcid.org/0000-0002-6606-5304; Email: stefano.passerini@kit.edu

Carsten Korte − *Institute of Energy and Climate Research, Electrochemical Process Engineering (IEK-14), Forschungszentrum Jülich GmbH, 52425 Jülich, Germany; Institute of Physical Chemistry, RWTH Aachen University, 52074 Aachen, Germany;* orcid.org/0000-0001-6574-6223; Email: c.korte@fz-juelich.de

Authors

Hui Hou − *Institute of Energy and Climate Research, Electrochemical Process Engineering (IEK-14), Forschungszentrum Jülich GmbH, 52425 Jülich, Germany; Institute of Physical Chemistry, RWTH Aachen University, 52074 Aachen, Germany;* orcid.org/0000-0003-1881-0573

Alessandro Mariani − *Helmholtz Institute Ulm (HIU), 89081 Ulm, Germany; Karlsruhe Institute of Technology (KIT), 76021 Karlsruhe, Germany;* orcid.org/0000-0002-3686-2169

Yanpeng Suo − *Institute of Energy and Climate Research, Electrochemical Process Engineering (IEK-14), Forschungszentrum Jülich GmbH, 52425 Jülich, Germany; Institute of Physical Chemistry, RWTH Aachen University, 52074 Aachen, Germany;* orcid.org/0000-0002-1108-6132

Xinpei Gao − *Helmholtz Institute Ulm (HIU), 89081 Ulm, Germany; Karlsruhe Institute of Technology (KIT), 76021 Karlsruhe, Germany*

Jürgen Giffin − *Institute of Energy and Climate Research, Electrochemical Process Engineering (IEK-14), Forschungszentrum Jülich GmbH, 52425 Jülich, Germany*
Christian Rodenbücher − *Institute of Energy and Climate Research, Electrochemical Process Engineering (IEK-14), Forschungszentrum Jülich GmbH, 52425 Jülich, Germany;* orcid.org/0000-0001-8029-3066

Complete contact information is available at: https://pubs.acs.org/10.1021/acs.chemmater.1c03819

Notes

The authors declare no competing financial interest.

■ ACKNOWLEDGMENTS

H.H., X.G., and A.M. acknowledge the financial support of the Federal Ministry for Economic Affairs and Energy (HiFi-PEFC, Project Number 03ETB003A). H.H. acknowledges T. Schubert from Iolitec GmbH for valuable suggestions relating to PIL synthesis. The authors are grateful to A. Mayer for carrying out the gel permeation chromatography experiment and to S. Willbold (ZEA-3) for performing the NMR experiments. H.H. is obliged to C. Wood for proofreading the manuscript. All authors are grateful for the support of the Helmholtz Association.

■ REFERENCES

(1) Sone, Y.; Ueno, M.; Naito, H.; Kuwajima, S. One kilowatt-class fuel cell system for the aerospace applications in a micro-gravitational and closed environment. *J. Power Sources* **2006**, *157*, 886−892.
(2) Kitahara, T.; Nakajima, H. Gas Diffusion Media and NaCl Contamination of Polymer Electrolyte Fuel Cells for Marine Applications. *ECS Trans.* **2018**, *86*, 271.
(3) Lin, B.; Qiu, L.; Lu, J.; Yan, F. Cross-linked alkaline ionic liquid-based polymer electrolytes for alkaline fuel cell applications. *Chem. Mater.* **2010**, *22*, 6718−6725.
(4) Jiang, S. P. Functionalized mesoporous structured inorganic materials as high temperature proton exchange membranes for fuel cells. *J. Mater. Chem. A* **2014**, *2*, 7637−7655.
(5) Peighambardoust, S. J.; Rowshanzamir, S.; Amjadi, M. Review of the proton exchange membranes for fuel cell applications. *Int. J. Hydrogen Energy* **2010**, *35*, 9349−9384.
(6) Bayer, T.; Cunning, B. V.; Selyanchyn, R.; Nishihara, M.; Fujikawa, S.; Sasaki, K.; Lyth, S. M. High temperature proton conduction in nanocellulose membranes: paper fuel cells. *Chem. Mater.* **2016**, *28*, 4805−4814.
(7) Van de Ven, E.; Chairuna, A.; Merle, G.; Benito, S. P.; Borneman, Z.; Nijmeijer, K. Ionic liquid doped polybenzimidazole membranes for high temperature proton exchange membrane fuel cell applications. *J. Power Sources* **2013**, *222*, 202−209.
(8) Appleby, A. Recent developments and applications of the polymer fuel cell. *Philos. Trans. R. Soc. Lond., Ser. A: Math., Phys. Eng. Sci.* **1996**, *354*, 1681−1693.
(9) Litster, S.; McLean, G. PEM fuel cell electrodes. *J. Power Sources* **2004**, *130*, 61−76.
(10) Jiao, K.; Alaefour, I. E.; Li, X. Three-dimensional non-isothermal modeling of carbon monoxide poisoning in high temperature proton exchange membrane fuel cells with phosphoric acid doped polybenzimidazole membranes. *Fuel* **2011**, *90*, 568−582.
(11) Li, Q.; Jensen, J. O.; Savinell, R. F.; Bjerrum, N. J. High temperature proton exchange membranes based on polybenzimidazoles for fuel cells. *Prog. Polym. Sci.* **2009**, *34*, 449−477.
(12) Lobato, J.; Canizares, P.; Rodrigo, M.; Linares, J.; Aguilar, J. Improved polybenzimidazole films for H3PO4-doped PBI-based high temperature PEMFC. *J. Membr. Sci.* **2007**, *306*, 47−55.
(13) Martinez, M.; Molmeret, Y.; Cointeaux, L.; Iojoiu, C.; Leprêtre, J.-C.; El Kissi, N.; Judeinstein, P.; Sanchez, J.-Y. Proton-conducting ionic liquid-based Proton Exchange Membrane Fuel Cell membranes: The key role of ionomer−ionic liquid interaction. *J. Power Sources* **2010**, *195*, 5829−5839.
(14) Lim, S. Y.; Martin, S.; Gao, G.; Dou, Y.; Simonsen, S. B.; Jensen, J. O.; Li, Q.; Norrman, K.; Jing, S.; Zhang, W. Self-Standing Nanofiber Electrodes with Pt−Co Derived from Electrospun Zeolitic Imidazolate Framework for High Temperature PEM Fuel Cells. *Adv. Funct. Mater.* **2021**, *31*, No. 2006771.
(15) Reimer, U.; Ehlert, J.; Janßen, H.; Lehnert, W. Water distribution in high temperature polymer electrolyte fuel cells. *Int. J. Hydrogen Energy* **2016**, *41*, 1837−1845.
(16) Maximini, M.; Engelhardt, P.; Brenner, M.; Beckmann, F.; Moritz, O. Fast start-up of a diesel fuel processor for PEM fuel cells. *Int. J. Hydrogen Energy* **2014**, *39*, 18154−18163.
(17) Wang, J.-T.; Savinell, R.; Wainright, J.; Litt, M.; Yu, H. A H2O2 fuel cell using acid doped polybenzimidazole as polymer electrolyte. *Electrochim. Acta* **1996**, *41*, 193−197.
(18) Wainright, J. S.; Wang, J. T.; Weng, D.; Savinell, R.; Litt, M. Acid-doped polybenzimidazoles: a new polymer electrolyte. *J. Electrochem. Soc.* **1995**, *142*, L121.
(19) Zhai, Y.; Zhang, H.; Zhang, Y.; Xing, D. A novel H3PO4/Nafion−PBI composite membrane for enhanced durability of high temperature PEM fuel cells. *J. Power Sources* **2007**, *169*, 259−264.
(20) Savadogo, O. Emerging membranes for electrochemical systems: Part II. High temperature composite membranes for polymer electrolyte fuel cell (PEFC) applications. *J. Power Sources* **2004**, *127*, 135−161.
(21) Mecerreyes, D.; Grande, H.; Miguel, O.; Ochoteco, E.; Marcilla, R.; Cantero, I. Porous polybenzimidazole membranes doped with phosphoric acid: highly proton-conducting solid electrolytes. *Chem. Mater.* **2004**, *16*, 604−607.
(22) Schuster, M. F.; Meyer, W. H. Anhydrous proton-conducting polymers. *Annu. Rev. Mater. Res.* **2003**, *33*, 233−261.
(23) Li, Q.; He, R.; Jensen, J.; Bjerrum, N. PBI-based polymer membranes for high temperature fuel cells−preparation, characterization and fuel cell demonstration. *Fuel Cells* **2004**, *4*, 147−159.
(24) Zelenay, P.; Scharifker, B.; Bockris, J. M.; Gervasio, D. A Comparison of the Properties of CF 3 SO 3 H and H 3 PO 4 in Relation to Fuel Cells. *J. Electrochem. Soc.* **1986**, *133*, 2262−2267.
(25) Murthi, V. S.; Urian, R. C.; Mukerjee, S. Oxygen reduction kinetics in low and medium temperature acid environment: correlation of water activation and surface properties in supported Pt and Pt alloy electrocatalysts. *J. Phys. Chem. B* **2004**, *108*, 11011−11023.
(26) Hsueh, K.-L.; Gonzalez, E.; Srinivasan, S. Electrolyte effects on oxygen reduction kinetics at platinum: a rotating ring-disc electrode analysis. *Electrochim. Acta* **1983**, *28*, 691−697.
(27) Wippermann, K.; Wackerl, J.; Lehnert, W.; Huber, B.; Korte, C. 2-Sulfoethylammonium trifluoromethanesulfonate as an ionic liquid for high temperature PEM fuel cells. *J. Electrochem. Soc.* **2016**, *163*, F25−F37.
(28) Compañ, V.; Escorihuela, J.; Olvera, J.; García-Bernabé, A.; Andrio, A. Influence of the anion on diffusivity and mobility of ionic liquids composite polybenzimidazol membranes. *Electrochim. Acta* **2020**, *354*, No. 136666.
(29) Lee, S.-Y.; Ogawa, A.; Kanno, M.; Nakamoto, H.; Yasuda, T.; Watanabe, M. Nonhumidified intermediate temperature fuel cells using protic ionic liquids. *J. Am. Chem. Soc.* **2010**, *132*, 9764−9773.
(30) Le Bideau, J.; Viau, L.; Vioux, A. Ionogels, ionic liquid based hybrid materials. *Chem. Soc. Rev.* **2011**, *40*, 907−925.
(31) Bao, X.; Zhang, F.; Liu, Q. Sulfonated poly (2, 5-benzimidazole)(ABPBI)/MMT/ionic liquids composite membranes for high temperature PEM applications. *Int. J. Hydrogen Energy* **2015**, *40*, 16767−16774.
(32) Skorikova, G.; Rauber, D.; Aili, D.; Martin, S.; Li, Q.; Henkensmeier, D.; Hempelmann, R. Protic ionic liquids immobilized in phosphoric acid-doped polybenzimidazole matrix enable polymer electrolyte fuel cell operation at 200 °C. *J. Membr. Sci.* **2020**, *608*, No. 118188.

(33) Nair, M. G.; Mohapatra, S. R. Perchloric acid functionalized nano-silica and protic ionic liquid based non-aqueous proton conductive polymer electrolytes. *Mater. Lett.* **2019**, *251*, 148−151.
(34) Wang, J. T.-W.; Hsu, S. L.-C. Enhanced high-temperature polymer electrolyte membrane for fuel cells based on polybenzimidazole and ionic liquids. *Electrochim. Acta* **2011**, *56*, 2842−2846.
(35) Neves, L. A.; Benavente, J.; Coelhoso, I. M.; Crespo, J. G. Design and characterisation of Nafion membranes with incorporated ionic liquids cations. *J. Membr. Sci.* **2010**, *347*, 42−52.
(36) Vázquez-Fernández, I.; Raghibi, M.; Bouzina, A.; Timperman, L.; Bigarré, J.; Anouti, M. Protic Ionic liquids/poly (vinylidene fluoride) composite membranes for fuel cell application. *J. Energy Chem.* **2021**, *53*, 197−207.
(37) Sood, R.; Iojoiu, C.; Espuche, E.; Gouanvé, F.; Gebel, G.; Mendil-Jakani, H.; Lyonnard, S.; Jestin, J. Comparative Study of Proton Conducting Ionic Liquid Doped Nafion Membranes Elaborated by Swelling and Casting Methods: Processing Conditions, Morphology, and Functional Properties. *J. Phys. Chem. C* **2014**, *118*, 14157−14168.
(38) Wippermann, K.; Suo, Y.; Korte, C. Oxygen Reduction Reaction Kinetics on Pt in Mixtures of Proton-Conducting Ionic Liquids and Water: The Influence of Cation Acidity. *J. Phys. Chem. C* **2021**, *125*, 4423−4435.
(39) Hou, H.; Schütz, H. M.; Giffin, J.; Wippermann, K.; Gao, X.; Mariani, A.; Passerini, S.; Korte, C. Acidic Ionic Liquids Enabling Intermediate Temperature Operation Fuel Cells. *ACS Appl. Mater. Interfaces* **2021**, *13*, 8370−8382.
(40) Hou, H.; Schütz, H. M.; Giffin, J.; Wippermann, K.; Gao, X.; Mariani, A.; Passerini, S.; Korte, C. Correction to "Acidic Ionic Liquids Enabling Intermediate Temperature Operation Fuel Cells". *ACS Appl. Mater. Interfaces* **2021**, *13*, 26649−26650.
(41) Karlsson, C.; Strietzel, C.; Huang, H.; Sjödin, M.; Jannasch, P. Nonstoichiometric triazolium protic ionic liquids for all-organic batteries. *ACS Appl. Energy Mater.* **2018**, *1*, 6451−6462.
(42) Khan, A.; Lu, X.; Aldous, L.; Zhao, C. Oxygen reduction reaction in room temperature protic ionic liquids. *J. Phys. Chem. C* **2013**, *117*, 18334−18342.
(43) Shoup, D.; Szabo, A. Chronoamperometric current at finite disk electrodes. *J. Electroanal. Chem. Interfacial Electrochem.* **1982**, *140*, 237−245.
(44) Huang, X.-J.; Rogers, E. I.; Hardacre, C.; Compton, R. G. The reduction of oxygen in various room temperature ionic liquids in the temperature range 293−318 K: Exploring the applicability of the Stokes− Einstein relationship in room temperature ionic liquids. *J. Phys. Chem. B* **2009**, *113*, 8953−8959.
(45) Bose, S.; Kuila, T.; Nguyen, T. X. H.; Kim, N. H.; Lau, K.-t.; Lee, J. H. Polymer membranes for high temperature proton exchange membrane fuel cell: recent advances and challenges. *Prog. Polym. Sci.* **2011**, *36*, 813−843.
(46) Wippermann, K.; Giffin, J.; Korte, C. In Situ determination of the water content of ionic liquids. *J. Electrochem. Soc.* **2018**, *165*, H263.
(47) Meister, E. C.; Willeke, M.; Angst, W.; Togni, A.; Walde, P. Confusing Quantitative Descriptions of Brønsted Lowry Acid Base Equilibria in Chemistry Textbooks−A Critical Review and Clarifications for Chemical Educators. *Helv. Chim. Acta* **2014**, *97*, 1−31.
(48) Lin, J.; Korte, C. Influence of the acid−base stoichiometry and residual water on the transport mechanism in a highly-Brønsted-acidic proton-conducting ionic liquid. *RSC Adv.* **2020**, *10*, 42596−42604.
(49) Corkum, R.; Milne, J. The density, electrical conductivity, freezing point, and viscosity of mixtures of trifluoromethanesulfonic acid and water. *Can. J. Chem.* **1978**, *56*, 1832−1835.
(50) Goodwin, S. E.; Smith, D. E.; Gibson, J. S.; Jones, R. G.; Walsh, D. A. Electroanalysis of neutral precursors in protic ionic liquids and synthesis of high-ionicity ionic liquids. *Langmuir* **2017**, *33*, 8436−8446.
(51) Scharifker, B. R.; Zelenay, P.; Bockris, J. M. The kinetics of oxygen reduction in molten phosphoric acid at high temperatures. *J. Electrochem. Soc.* **1987**, *134*, 2714−2725.
(52) Bouchet, R.; Siebert, E. Proton conduction in acid doped polybenzimidazole. *Solid State Ionics* **1999**, *118*, 287−299.
(53) Shen, C.-H.; Hsu, S. L.-c.; Bulycheva, E.; Belomoina, N. Polybenzimidazole/1H-imidazole-4-sulfonic acid hybrid membranes for high-temperature proton exchange membranes fuel cells. *J. Membr. Sci.* **2012**, *399−400*, 11−15.
(54) Lin, J.; Korte, C. PBI-type Polymers and Acidic Proton Conducting Ionic Liquids−Conductivity and Molecular Interactions. *Fuel Cells* **2020**, *20*, 461−468.
(55) Asensio, J. A.; Sánchez, E. M.; Gómez-Romero, P. Proton-conducting membranes based on benzimidazole polymers for high-temperature PEM fuel cells. A chemical quest. *Chem. Soc. Rev.* **2010**, *39*, 3210−3239.
(56) Johnston, D. H.; Shriver, D. F. Vibrational study of the trifluoromethanesulfonate anion: unambiguous assignment of the asymmetric stretching modes. *Inorg. Chem.* **1993**, *32*, 1045−1047.
(57) De Angelis, A.; Flego, C.; Ingallina, P.; Montanari, L.; Clerici, M.; Carati, C.; Perego, C. Studies on supported triflic acid in alkylation. *Catal. Today* **2001**, *65*, 363−371.
(58) Wang, X.; Wang, S.; Liu, C.; Li, J.; Liu, F.; Tian, X.; Chen, H.; Mao, T.; Xu, J.; Wang, Z. Cage-like cross-linked membranes with excellent ionic liquid retention and elevated proton conductivity for HT-PEMFCs. *Electrochim. Acta* **2018**, *283*, 691−698.
(59) Ghosh, S.; Maity, S.; Jana, T. Polybenzimidazole/silica nanocomposites: Organic-inorganic hybrid membranes for PEM fuel cell. *J. Mater. Chem.* **2011**, *21*, 14897−14906.
(60) Ogungbemi, E.; Ijaodola, O.; Khatib, F.; Wilberforce, T.; El Hassan, Z.; Thompson, J.; Ramadan, M.; Olabi, A. Fuel cell membranes−Pros and cons. *Energy* **2019**, *172*, 155−172.
(61) Arias, J. J. R.; Dutra, J. C.; de Souza Gomes, A. Hybrid membranes of sulfonated poly ether ether ketone, ionic liquid and organically modified montmorillonite for proton exchange membranes with enhanced ionic conductivity and ionic liquid lixiviation protection. *J. Membr. Sci.* **2017**, *537*, 353−361.
(62) Kreuer, K.-D. Ion conducting membranes for fuel cells and other electrochemical devices. *Chem. Mater.* **2014**, *26*, 361−380.
(63) Kuroha, M.; Gotoh, H.; Miran, M. S.; Yasuda, T.; Watanabe, M.; Sakakibara, K. Proton-conductivity-enhancing Ionic Liquid consisting of guanidine and excess trifluoromethanesulfonic acid. *Chem. Lett.* **2014**, *43*, 649−651.
(64) He, R.; Li, Q.; Bach, A.; Jensen, J. O.; Bjerrum, N. J. Physicochemical properties of phosphoric acid doped polybenzimidazole membranes for fuel cells. *J. Membr. Sci.* **2006**, *277*, 38−45.
(65) McLean, R. S.; Sauer, B. B. Tapping-mode AFM studies using phase detection for resolution of nanophases in segmented polyurethanes and other block copolymers. *Macromolecules* **1997**, *30*, 8314−8317.
(66) Bai, H.; Wang, H.; Zhang, J.; Zhang, J.; Lu, S.; Xiang, Y. High temperature polymer electrolyte membrane achieved by grafting poly (1-vinylimidazole) on polysulfone for fuel cells application. *J. Membr. Sci.* **2019**, *592*, No. 117395.
(67) Fujimura, M.; Hashimoto, T.; Kawai, H. Small-angle X-ray scattering study of perfluorinated ionomer membranes. 2. Models for ionic scattering maximum. *Macromolecules* **1982**, *15*, 136−144.
(68) Gebel, G.; Lambard, J. Small-angle scattering study of water-swollen perfluorinated ionomer membranes. *Macromolecules* **1997**, *30*, 7914−7920.
(69) Kannan, R.; Kagalwala, H. N.; Chaudhari, H. D.; Kharul, U. K.; Kurungot, S.; Pillai, V. K. Improved performance of phosphonated carbon nanotube−polybenzimidazole composite membranes in proton exchange membrane fuel cells. *J. Mater. Chem.* **2011**, *21*, 7223−7231.
(70) Dominguez, P. H.; GrygielK, K.; Weber, J. Nanostructured poly (benzimidazole) membranes by N-alkylation. *Express Polym. Lett.* **2014**, *8*, 30−38.